INSTITUT D'AERONOMIE SPATIALE DE BELGIQUE

3 - Avenue Circulaire
B - 1180 BRUXELLES

AERONOMICA ACTA

A - N° 164 - 1976

Diamagnetic boundary layers: a kinetic theory

by

J. LEMAIRE and L.F. BURLAGA

BELGISCH INSTITUUT VOOR RUIMTE-AERONOMIE

3 - Ringlaan
B - 1180 BRUSSEL

FOREWORD

The article "Diamagnetic Boundary layers : A kinetic theory" has been prepared when one of the authors (J.L.) was a NAS-NRC Research Associate at NASA- Goddard Space Flight Center, Greenbelt, Md. This article will be published in *Astrophysics and Space Science*.

AVANT-PROPOS

L'article intitulé "Diamagnetic Boundary layers : A kinetic theory" a été réalisé grâce à la National Academy of Sciences - National Research Council qui a subsidié un séjour de six mois pour l'un des auteurs (J.L.) au NASA-Goddard Space Flight Center, Greenbelt, Md.. USA. L'article sera publié dans *Astrophysics and Space Science*.

VOORWOORD

Het artikel "Diamagnetic Boundary Layers : A kinetic theory" is tot stand gekomen dank zij de National Academy of Sciences - National Research Council die aan een van de schrijvers (J.L.) een toelage voor een verblijf van zes maanden heeft verzekerd aan het NASA-Goddard Space Flight Center, Greenbelt, Md., USA. Het artikel zal verschijnen in *Astrophysics and Space Science*.

VORWORT

Das Artikel "Diamagnetic Boundary Layers : A kinetic theory" wurde mit der Bestüzung der National Academy of Sciences - National Research Council entworfen als einer der Verfasser (J.L.) während sechs Monate in NASA- Goddard Space Flight Center war, Greenbelt, Md., USA. Dieses Artikel wir in *Astrophysics and Space Science* veröffendlicht.

DIAMAGNETIC BOUNDARY LAYERS : A KINETIC THEORY

by

J. LEMAIRE* and L.F. BURLAGA**

* *Institut d'Aéronomie Spatiale de Belgique, B-1180 Bruxelles*
** *Goddard Space Flight Center, Greenbelt, Md., U.S.A.*

Abstract

We present a kinetic theory for boundary layers associated with MHD tangential 'discontinuities' in a collisionless magnetized plasma such as those observed in the solar wind. The theory consists of finding self-consistent solutions of Vlasov's equation and Maxwell's equation for stationary, one-dimensional boundary layers separating two Maxwellian plasma states. Layers in which the current is carried by electrons are found to have a thickness of the order of a few electron gyroradii, but the drift speed of the current-carrying electrons is found to exceed the Alfvén speed, and accordingly such layers are not stable. Several types of layers, in which the current is carried by protons are discussed; in particular, we considered cases in which the magnetic field intensity and/or direction changed across the layer. In every case, the thickness was of the order of a few proton gyroradii and the field changed smoothly, although the characteristics depended somewhat on the boundary conditions. The drift speed was always less than the Alfvén speed, consistent with stability of such structures. Our results are consistent with the observations of boundary layers in the solar wind near 1 AU.

Résumé

Un modèle cinétique est proposé pour décrire les discontinuités tangentielles dans le vent solaire. Les solutions données satisfont aux équations de Vlasov et de Maxwell et décrivent des couches de courants diamagnétiques séparant deux plasma ayant des densités et températures différentes. L'épaisseur de ces couches limites est soit de l'ordre de quelques rayons de gyration des électrons, soit de l'ordre de quelques rayons de gyration des ions. L'un ou l'autre type de structure prévaut suivant que le courant diamagnétique est transporté par les électrons ou seulement par les ions. Les modèles particuliers choisis pour illustrer la théorie correspondent à des structures semblables à celles qui sont observées dans le vent solaire à 1 U.A.

Samenvatting

Een kinetisch model, dat de tangentiele discontinuiteiten in de zonnewind beschrijft, wordt voorgesteld. De gegeven oplossingen voldoen aan de vergelijkingen van Vlasov en Maxwell en beschrijven lagen van diamagnetische stromen die twee plasma met verschillende dichtheid en temperatuur scheiden. De dikte van deze limietlagen is ofwel van de grootte-orde van enkele gyratiestralen van de electronen ofwel van enkele gyratiestralen van de ionen. Het ene of het andere structuurtype wordt aangenomen naargelang de diamagnetische stroom overgebracht wordt door de electronen of enkel door de ionen. De afzonderlijke modellen die gekozen werden om de theorie de staven stemmen overeen met structuren gelijkaardig aan deze die in de zonnewind werden waargenomen op 1 U.A.

Zusammenfassung

Ein kinetisches Model für tangentialle Diskontinuitäte ist vorgeschagen worden. Die Auflösungen der Vlasov und Maxwell Gleichungen beschreiben diamagnetische Ströme die zwei Plasmas mit verschiedene Dichten und Temperaturen abteilen. Die Breiten dieser Schichten ist entweder einige Electron Larmor Radius or einige Ionen Larmor Radius, dem nach dass die electrisch-diamagnetische Ströme durch die Electronen order nur durch die Ionen übertragen sind. Die bestimmte Modelle die hier forgeschlagen sindum die Theorie zu illustrieren, sind den tangentiallen Diskontinuitäten des Sonnen Windes ähnlich.

1. INTRODUCTION

Observations of MHD 'discontinuities' in the solar wind have been discussed in many papers and were reviewed by Burlaga (1971, 1972) and Siscoe (1974). However, only a few papers (Siscoe *et al.*, 1968; Burlaga, 1969; Smith, 1973) have discussed the structure of the current sheets associated with such discontinuities, and these were limited by the time resolution of the observations and failure to include plasma observations. The current sheets are quite thin. For example, Siscoe *et al.*, (1968) showed that they are generally convected past a 'fixed' S/C in less than 10 s and thus have dimensions $\lesssim$ 10 proton Larmor radii, a_L. They are 'kinetic-scale' phenomena, in the classification scheme of Burlaga (1969), and one expects that a kinetic theory is needed to describe them.

The observations of current sheets, which are referred to above, do not have sufficient time resolution to allow one to study the structure of the thinnest sheets or obtain the most probable thickness. For example, the structures exhibited by Smith (1973), Siscoe *et al.* (1968) and Burlaga (1969) had a width of $\approx$ 1 min. Consequently, the results are not representative of current sheets in general.

Magnetic field observations from the GSFC magnetometer on IMP I have a sampling rate of $\approx 14\ s^{-1}$, an order of magnitude improvement over the rates discussed above, and have clearly resolved the structure of even the thinnest current sheets. Simultaneous plasma measurements are also available, although their time resolution is rather poor. These observations are discussed in a companion paper (Burlaga *et al.*, 1976). Here, our aim is to understand these structures. The emphasis is on the theory itself.

The theory which we present is an extension of the work of Sestero (1964) on the structure of plasma sheaths. Sestero considers only the case in which the magnitude of B changes while the direction does not. This does not frequently occur in the solar wind. The most likely configuration is a change in the direction of B with no change in magnitude, but one also observes changes in both $|\mathbf{B}|$ and $\hat{\mathbf{B}}$ in interplanetary sheaths. Thus, our work concerns the generalization of Sestero's theory to include both changes in $|\mathbf{B}|$ and $\hat{\mathbf{B}}$. It also

includes changes in composition, temperature anisotropy, etc. Alpers (1969, 1971) has discussed current sheets, but he assumed zero electric fields, whereas we let $\mathbf{E} \neq 0$. Stern (1975) has discussed particle trapping at discontinuities.

The significance of this work extends beyond a discussion of the sheaths themselves. It represents a new theoretical framework for discussing kinetic scale phenomena in the solar wind. The starting point is the Vlasov equation as opposed to the fluid equations which have been used to discuss processes on a larger scale.

2. BASIC EQUATIONS AND ASSUMPTIONS

2.1. Field equations

Since the solar wind speeds before and after tangential discontinuities are usually more or less the same, it can be considered with some confidence that tangential discontinuities are steady-state structures convected with the solar wind velocity - i.e., (1) that the projection of **W** the plasma bulk velocity along **N** the normal to the current sheath is the same on both sides of the discontinuity ($\mathbf{W}_l.\mathbf{N} = \mathbf{W}_r.\mathbf{N}$), and (2) that their thickness doesn't change significantly in a time comparable to that during which they are observed at 1 AU. Therefore, in the frame of reference moving with the solar wind the steady-state field equations are, in rationalized MKS units,

$$\text{curl } \mathbf{B} = \mu_o \sum_i Z_i e \mathbf{F}_i \tag{2.1}$$

$$\mathbf{B} = \text{curl } \mathbf{A} \tag{2.2}$$

$$\text{div } (\epsilon_o \mathbf{E}) = \sum_i Z_i e n_i \tag{2.3}$$

$$\mathbf{E} = - \text{grad } \phi \tag{2.4}$$

where **A** and ϕ are the vector and scalar potentials of the magnetic field **B** and electric field **E**, respectively; μ_o and ϵ_o are the permeability and permittivity of free space; $Z_i e$, $\mathbf{F}_i$ and n_i

are respectively the electric charge, flux, and number density of the particle species i, where i stands for e (electron), p (proton), α (alpha particle).

It will also be assumed that the curvature of the current sheath is small compared to its thickness. Some evidence which supports this was given by Burlaga and Ness (1969). As a consequence it can be considered (1) that the surface of discontinuity is a plane, and (2) that all quantities depend on x, the space coordinate along $\hat{N}$, the unit vector normal to this plane (see Figure 1). It results from these assumptions that

$$E_y = \text{const}, \qquad E_z = \text{const}, \qquad B_x = \text{const}. \tag{2.5}$$

Since we don't examine rotational discontinuities but only the commonly observed tangential discontinuities, we can set $B_x = 0$.

Furthermore, since it was assumed that there is no mass flux normal to the surface of discontinuity (as would be the case of a shock front or rotational discontinuity) $W_x = 0$ implies that

$$E_y B_z - E_z B_y = 0 . \tag{2.6}$$

If we consider that the electric conductivity is very large along the magnetic field direction, there can be no significant electric field parallel to B - i.e.,

$$E_y B_y + E_z B_z = 0 . \tag{2.7}$$

From (2.6) and (2.7) we obtain, in the frame of reference moving with the solar wind, $E_z = 0$ and $E_y = 0$. In the paper of Sestero (1964) the magnetic field remains parallel to the z-axis - i.e., $B_y = 0$. To allow for a change in the direction of the magnetic field across the current sheath we shall consider the slightly more general situation where both B_z and B_y are functions of x and solutions of the equations

$$\frac{dB_y}{dx} = \mu_o \sum_i Z_i e F_{z,i} \quad . \tag{2.8}$$

$$\frac{dB_z}{dx} = -\mu_o \sum_i Z_i e F_{y,i} \quad . \tag{2.9}$$

$$\frac{dA_z}{dx} = -B_y \quad . \tag{2.10}$$

$$\frac{dA_y}{dx} = B_z \quad . \tag{2.11}$$

with the boundary conditions

$$\lim_{x \to l} B_y = B_l \sin \phi_l \quad . \tag{2.12}$$

$$\lim_{x \to l} B_z = B_l \cos \phi_l \quad . \tag{2.13}$$

where B_l is the intensity of the magnetic field on the left-hand side at $x = x_l$, and ϕ_l the angle of B and the z-axis (see Figure 1).

It is convenient to determine the z-axis such that B_y is negative or zero, and B_z is positive at $x = x_l$: i.e., $-90^0 < \phi_l < 0$. In such a coordinate system A_z and A_y are both increasing functions of x such that

$$\lim_{x \to -\infty} A_y = -\infty \quad \text{and} \quad \lim_{x \to -\infty} A_z = -\infty \quad . \tag{2.14}$$

The electric field equations (2.3) and (2.4) become

$$\frac{dE_x}{dx} = \frac{1}{\epsilon_o} \sum_i Z_i e n_i \quad . \tag{2.15}$$

$$\frac{d\phi}{dx} = - E_x \; ; \tag{2.16}$$

with the boundary conditions

$$\lim_{x \to -\infty} \phi = 0 \tag{2.17}$$

and

$$\lim_{x \to -\infty} E_x = 0 . \tag{2.18}$$

The condition (2.18) implies that, except inside the narrow current sheath, the drift velocity ($\mathbf{E} \times \mathbf{B}/B^2$) and the fluxes $\mathbf{F}_i$ become vanishingly small when $x \to -\infty$.

If the electric current and charge density, or the fluxes, F_i, and concentrations, n_i, are known functions of x and/or A_y, A_z, ϕ, the set of differential equations (2.8)-(2.11), (2.15)-(2.16) can in principle be integrated to determine the distribution of the field variables B_y, B_z, E_x, A_y A_z, ϕ.

In the next section we show how it is possible to determine such functions

$$n_i = Q_i^{000}(\phi, A_y, A_z) , \tag{2.19}$$

$$F_{y,i} = Q_i^{010}(\phi, A_y, A_z) , \tag{2.20}$$

$$F_{z,i} = Q_i^{001}(\phi, A_y, A_z) , \tag{2.21}$$

where $Q_i^{sm\,n}$ are the moments of the velocity distributions $f_i(v, x)$

$$Q_i^{sm\,n} = \iiint_{-\infty}^{\infty} v_x^s v_y^m v_z^n f_i(v,x)\, dv. \tag{2.22}$$

2.2. The plasma equations

The densities and fluxes in the right-hand side of equations (2.8), (2.9) and (2.15) are the zero and first order moments of the velocity distribution, Equations (2.19)-(2.21). These quantities must be solutions of the steady-state transport equations - i.e., the continuity equation

$$\frac{d(n_i W_{x,i})}{d_x} = 0 ; \quad \text{or} \quad \frac{dF_{x,i}}{dx} = 0 . \tag{2.23}$$

This equation is necessarily satisfied in our case since the flux, F_x, and the bulk velocity, W_x, normal to the surface of discontinuity are assumed to be zero for each species.

The equations of motion are

$$\frac{d}{dx} p_{xy,i} = 0 , \tag{2.24}$$

$$\frac{d}{dx} p_{xz,i} = 0 , \tag{2.25}$$

$$\frac{d}{dx} p_{xy,i} = Z_i e(n_i E_x + F_{y,i} B_z - F_{z,i} B_y) , \tag{2.26}$$

where $p_{xy,i}$, $p_{xz,i}$ and $p_{xx,i}$ are components of the kinetic pressure tensor defined by Q_i^{110}, Q_i^{101} and Q_i^{200} respectively (Equation 2.22).

Note that the usual total pressure balance equation can be obtained from (2.26) by summing for all species, and by using (2.8), (2.9) and (2.15) to replace $\Sigma_i Z_i e F_{y,i}$, $\Sigma_i Z_i e F_{z,i}$ and $\Sigma_i Z_i$ en $_i$: i.e.,

$$\frac{d}{dx} \left(\sum_i p_{xx,i} + \frac{B_y^2 + B_z^2}{2\mu_o} + \frac{\epsilon_o}{2} E_x^2 \right) = 0. \tag{2.27}$$

Note the presence of the term E_x^2.

When collisions are sufficiently frequent to maintain an isotropic and Maxwellian velocity distribution with a temperature T_i, the transport equations can easily be closed by introducing some additional assumptions - e.g., isotropic pressure ($p_{xy,i} = P_{yz,i} = p_{xz,i} = 0$, $p_{xx,i} = p_{yy,i} = p_{zz,i} = n_i k T_i$) with a constant or polytropic temperature distribution. Other classical hydrodynamic approximations as, for instance, the Navier-Stokes relations, are sometimes used when viscosity and conductivity become more important, and when the mean free path of the particles can no longer be considered as infinitely small.

In the opposite limit, when the average mean free path of the particles becomes large compared to the characteristic dimension of the system. we cannot, as in the collision dominated regime, define relevant relationships between the higher and lower order moments of the velocity distributions. As a consequence there is no obvious method to close the system of transport equations, and we are led to step back to Liouville's or Vlasov's equation of the form

$$v_x \frac{\partial f_i}{\partial x} + \frac{Z_i e}{m_i} \left[(E_x + v_y B_z - v_z B_y) \frac{\partial f_i}{\partial v_x} - v_x B_z \frac{\partial f_i}{\partial v_z} - v_x B_y \frac{\partial f_i}{\partial v_z} \right] = 0 \qquad (2.28)$$

It can be verified that any function of the constants of motion of the particles is a solution of Vlasov's equation. In a steady-state electromagnetic field as defined in Section 2.1 and illustrated in Figure 1, the constants of motion are the conjugate momenta of the space variables y and z - i.e.,

$$p_y = m_i v_y + Z_i e A_y \; , \qquad (2.29)$$

$$p_z = m_i v_z + Z_i e A_z \; ; \qquad (2.30)$$

and the total energy

$$W = \frac{1}{2} m_i (v_x^2 + v_y^2 + v_z^2) + Z_i e \phi \; . \qquad (2.31)$$

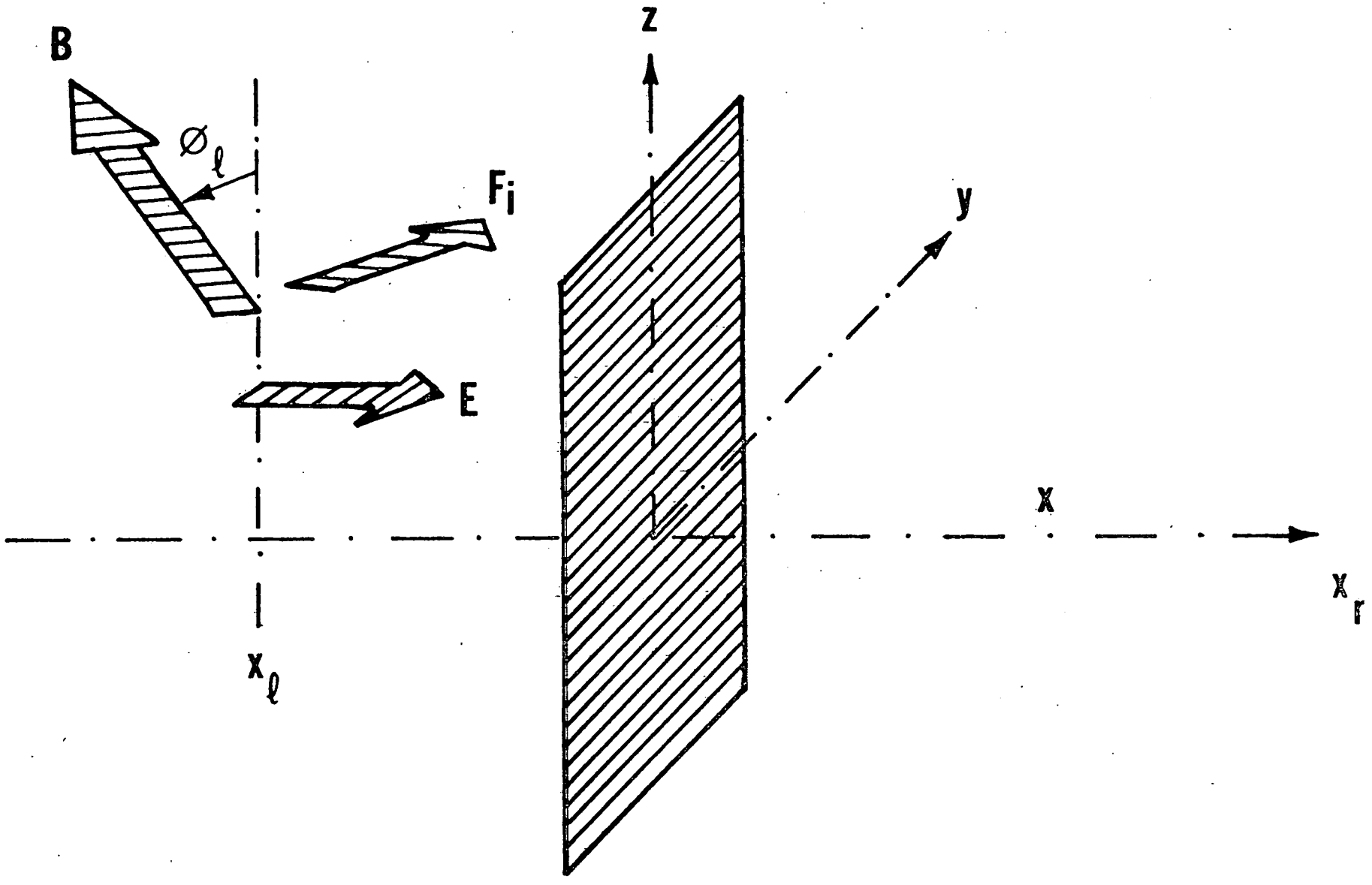

Fig. 1

Among the infinite number of possibilities, we have chosen a function $f_i(p_y, p_z, W)$ such that, in the limits $x \to \pm \infty$, f_i tends to the actual Maxwellian velocity distributions on the left- and right-hand sides of the surface of discontinuity: i.e.,

$$\lim_{x \to -\infty} f_i = N_l \left(\frac{m_i}{2\pi k T_{l,i}} \right)^{3/2} \exp \left(- \frac{mv^2}{2kT_{l,i}} \right) = f_{l,i}(v) , \tag{2.32}$$

$$\lim_{x \to +\infty} f_i = N_r \left(\frac{m_i}{2\pi k T_{r,i}} \right)^{3/2} \exp \left(- \frac{mv^2}{2kT_{r,i}} \right) = f_{r,i}(v) , \tag{2.33}$$

where $N_{l,i}$, $N_{r,i}$, $T_{l,i}$, $T_{r,i}$ are the number densities and kinetic temperatures of the particles, i, on the left (l) and right (r) side of the discontinuity.

The boundary conditions of $f_i(p_y, p_z, W)$ limit somewhat the choice of this arbitrary function of the constants of motion but not enough to determine it completely or uniquely. The reason for this indeterminacy is that in a collisionless regime it is always possible to add an arbitrary amount of 'trapped' particles which never can reach $x = \pm \infty$. This point has already been made by Stern (1975) using very general arguments. The velocity and pitch angle distributions of these 'trapped' particles are not determined by the boundary conditions at $x = \pm \infty$, at least in absence of collisions. We shall use for $f_i(p_y, p_z, W)$ the function

$$f_i = N_{l,i} \left(\frac{m_i}{2\pi k T_{l,i}} \right)^{3/2} \exp \left(- \frac{W}{kT_{l,i}} \right) \eta(-p_z)\, \eta(-p_y) +$$

$$+ N_{r,i} \left(\frac{m_i}{2\pi k T_{r,i}} \right)^{3/2} \exp \left(- \frac{W}{kT_{r,i}} \right) [1 - \eta(-p_z)\eta(-p_y)] , \tag{2.34}$$

where $\eta(p)$ is the step function ($\eta(p) = 0$ for $p < 0$ and $\eta(p) = 1$ for $p > 0$). This means that $f_i = f_{r,i} = N_{r,i}(m_i/2\pi k T_{r,i})^{3/2} \exp(-W/kT_{r,i})$ everywhere except in the quadrant $p_y < 0$, $p_z < 0$, where $f_i = f_{l,i}$. In terms of speeds, $f = f_{r,i}$ everywhere except in the region $V_y <$

$- Z_i eA_y/m_i$, $V_z < - Z_i eA_z/m_i$, where it equals $f_{l,i}$. Since $A_y \rightarrow -\infty$ and $A_z \rightarrow -\infty$ as $x \rightarrow -\infty$ (see 2.14), this means that $f \rightarrow f_{l,i}$ as $x \rightarrow -\infty$. Thus, the choice of (2.34) gives the desired transition from one Maxwellian state at $x = +\infty$ to another at $x = -\infty$. In the special case that $N_l = N_r$ and $T_l = T_r$, f_i is isotropic and Maxwellian at any distance x; this follows immediately from (2.34).

The function (2.34) is symmetrical with respect to the quadrants $p_y < 0$, $p_z > 0$ and $p_y > 0$, $p_z < 0$, but it is asymmetrical with respect to the quadrants $p_y > 0$, $p_z > 0$, and $p_y < 0$, $p_z < 0$. This asymmetry allows currents in any direction in the (V_y, V_z) plane : these must be chosen to be consistent with the specified directions of B at $x = \pm \infty$ and our sign conventions.

The expression (2.34) should not be considered as an exact representation of the actual velocity distribution, but as one possible solution of Vlasov's Equation (2.38) satisfying the boundary conditions (2.32) and (2.33). This solution is not unique. By this particular choice for f_i we describe only one set of structures among a much broader family of similar current sheaths. Our aim is to find a solution which describes the basic features of the observations, viz., the observed thickness and the laminar nature of the transition. One cannot expect the function (2.34) to describe the detailed structure of every tangential discontinuity. Nevertheless, one can calculate, self-consistently, a possible set of structures and determine their characteristic thickness.

In the Appendix we give the algebraic expressions for the moments of f_i; these moments $Q_i^{s\,m\,n}$ (Equation 2.22) satisfy the general transport equations and the boundary conditions at $x = \pm \infty$. The general formula for $Q_i^{s\,m\,n}$ given in the Appendix, can be used in the right-hand side of the field Equations (2.8)-(2.11), (2.15)-(2.16) to model the electric current and charge density distribution. The distribution of the electric and magnetic potentials and fields are finally determined by numerical integration of these differential equations. The method of integration and the description of the numerical solutions are given in the next section.

3. SUMMARY OF THE EQUATIONS AND THE METHOD OF SOLUTION

It is rather convenient to introduce non-dimensional variables and define the new units given in Table I. In this new unit system the equations are

$$\frac{dB_y}{dx} = \sum_i Z_i Q_i^{001} , \tag{3.1}$$

$$\frac{dB_z}{dx} = -\sum_i Z_i Q_i^{010} , \tag{3.2}$$

$$\frac{dA_z}{dx} = -B_y , \tag{3.3}$$

$$\frac{dA_y}{dx} = B_z , \tag{3.4}$$

$$\epsilon_o \mu_o \frac{kT_{l,e}}{m_e} \frac{d^2\phi}{dx^2} = -\sum_i Z_i Q_i^{000} . \tag{3.5}$$

Note that the RHS of (3.5) is the relative excess of electrons, or the charge separation density $(n_e - Z_{ion} n_{ion})/n_e$. In addition, one has the following relations which are obtained from (2.22) with $f = f(W(\phi, A_y, A_z), p(\phi, A_y, A_z))$ given by (2.34): i.e., $Q_i^{001} = Q_i^{001}(\phi, A_y, A_z)$, $Q_i^{010} = Q_i^{010}(\phi, A_y, A_z)$, and $Q_i^{000} = Q_i^{000}(\phi, A_y, A_z)$. Note the Q_i^{000} is the dimensionless density of the ith species, and Q_i^{001}, Q_i^{010} are the dimensionless currents carried by species i along $\hat{z}$ and $\hat{y}$, respectively. Thus, for a proton-electron plasma we have 11 equations for the 11 functions $B_y(x)$, $B_z(x)$, $A_y(x)$, $A_z(x)$, $\phi(x)$, $Q_e^{000}(x)$, $Q_e^{010}(x)$, $Q_e^{001}(x)$, $Q_{ion}^{000}(x)$, $Q_{ion}^{010}(x)$, and $Q_{ion}^{001}(x)$.

The solution of our system of equations is greatly simplified by noting that the right-hand side of (3.5) is generally small in usual circumstances. Indeed, unless the second derivative of the non-dimensional electric potential (or the variation of the electric field) is unreasonably large ($|d^2\phi/dx^2| > 10^4$), the charge separation density is of the order of

TABLE I : The New Units

The corresponding value in familiar units is given for $N_{l,e} = 5\ cm^{-3}$, $T_{l,e} = 1.5 \times 10^5$ K; k is the Boltzman Constant ; μ is the permeability of free space; m_e is the electron mass; e is the electron charge.

Variable	Symbol	New Unit	Value	
Density	$n_i; N_{r,i} \ldots$	$N_{l,e}$	5	cm^{-3}
Distance	x	$(m_e/\mu N_{l,e} e^2)^{1/2}$	2.37	km
Temperature	$T_i; T_{r,i} \ldots$	$T_{l,e}$	1.5×10^5	K
Velocity	$W_i; v_x \ldots$	$(2kT_{l,e}/m_e)^{1/2}$	2132	km x s^{-1}
Pressure	$p_{xy,i}; p_{xx,i}$	$2N_{l,e} kT_{l,e}$	2.07×10^{-10}	dyne x cm^{-2}
Particle Flux	$F_{y,i}; F_{z,i}$	$N_{l,e}(2kT_{l,e}/m_e)^{1/2}$	1.06×10^9	cm^{-2} x s^{-1}
Current Density	$J_{y,i}; J_{z,i}$	$eN_{l,e}(2kT_{l,e}/m_e)^{1/2}$	1.70×10^{-6}	amp x m^{-2}
Electric Potential	ϕ	$kT_{l,e}/e$	12.9	Volt
Electric Field	E_x	$(\mu k^2 T_{l,e} N_{l,e}/m_e)^{1/2}$	5.43	mV m^{-1}
Magnetic Induction	B_y ; B_z	$(2\mu kT_{l,e} N_{l,e})^{1/2}$	5.1	gamma
Vector Potential	$A_y; A_z$	$(2kT_{l,e} m_e/e)^{1/2}$	----	----
Heat Flux	$q_{y,i}; q_{z,i}$	$N_{l,e}(2kT_{l,e}/m_e)^{3/2}$	2.20×10^{-2}	erg x cm^{-2} x s^{-1}
Higher Order Moments	Q_i^{mni}	$N_{l,e}(2kT_{l,e}/m_e)^{\frac{m+n+1}{2}}$	---	----

TABLE II : Boundary Conditions

Figure No / Model No.			2 a	2 b	3 c	3 d	4 e	4 f	5 g	5 h	
Number density	$N_{l,e}$	(*)	5	5	5	5	5	5	5	5	cm^{-3}
	$N_{l,p}$	(*)	5	5	5	5	5	5	5	5	
	$N_{r,e}$	(*)	2.5	4.5	5	5	5	5	5	5	
	$N_{l,p}$	(*)	2.5	7.5	1	1	3.69	1	2.862	12.73	
Temperatures	$T_{l,e}$	(*)	1.5	1.5	1.5	1.5	1.5	1.5	1.5	1.5	10^5 K
	$T_{l,p}$	(*)	0.5	0.5	0.5	0.5	0.5	0.5	0.5	0.5	
	$T_{r,e}$	(*)	1.5	1.2	1.5	1.5	1.5	1.5	1.5	1.5	
	$T_{r,p}$	(*)	0.5	0.2	0.5	0.1	1	1	1	0.25	
Magnetic field intensity	B_l	(*)	2	2	2	2	2	2	2	2	Gamma
and angle at - ∞	ϕ_l	(*)	- 45	- 45	- 45	- 45	0	0	- 45	- 45	degree
Rotation parameter	ρ	(*)	1.5	0.8	0.8	0.8	∞	∞	0.5	0.5	
Electric potential difference	$\phi(\infty)$	(4.1)	0	0.0584	- 0.402	- 0.100	- 0.181	- 0.643	- 0.223	0.133	Dimensionless (see Table I)
Density at + ∞	$n_p(\infty)$	(4.2)	2.5	4.84	3.34	4.52	4.43	2.62	4.0	5.71	cm^{-3}
Magnetic field intensity	B_r	(calc.)	4.62	3.89	3.93	3.68	0.5	3.98	2.15	1.32	Gamma
and angle at x = + ∞	ϕ_r	(calc.)	- 18	- 63.3	- 64.2	- 63.1	0	0	- 54.8	- 36.4	degree

(*) are given as input ; (4.1) means that $\phi(\infty)$ is given by equation (4.1) ; (calc) means that this quantity is obtained from the numerical integration stopped at x = + ∞ : i.e., at a large distance from the current layer.

$\epsilon_o \mu_o k T_e / m_e$: i.e., the square of the electron thermal speed divided by the square of the velocity of light; for $T_e = 1.5 \times 10^5$K the charge separation density $(n_e - Z_{ion} n_{ion})/ n_e$ is less than (2-3) x 10^{-5}. Under normal conditions it is expected that the right-hand side of Equation (3.5) is always very small and that the quasi-neutrality condition is satisfied. This implies that under normal circumstances the electric potential ϕ can be calculated by solving the algebraic equation

$$\sum_i Z_i Q_i^{000}(\phi, A_y, A_z) = 0 , \qquad (3.6)$$

instead of integrating the non-linear differential Equation (3.5). In other words, the electric potential is adjusted to have an electron density distribution $n_e(x)$ exactly equal to the total ion charge density in the presence of the potential A(x). One thus obtains an equation for $\phi(A_y, A_z)$. Given $\phi(A_y(x), A_z(x))$, one can calculate $E_x = - d\phi/dx$ and one can verify a posteriori that $d^2\phi/dx^2$ and $\Delta n/n$ are negligibly small.

Our equations reduce to those of Sestero (1964) if we set $T_{l,i} = T_{r,i}$ = constant, $T_{l,e} = T_{r,e}$ = constant and $A_z = 0$. In other words, Sestero considered the special case of an isothermal boundary layer with $\mathbf{B}_r$ parallel (or antiparallel) to $\mathbf{B}_l$. In this case one obtains an *analytical* expression for $\phi(A_y)$ by setting the RHS of (3.5) equal to zero (Sestero, 1964; Equation 19). Equations (3.3) and (3.1) do not enter since $B_y = A_z = 0$ by assumption. Integrating the distribution function with $\phi = \phi(A_y)$ gives analytical expressions for $Q_e^{010}(A_y)$ and $Q_{ion}^{010}(A_y)$ (Sestero, 1964; Equation 17) which may be substituted into the RHS of (3.2). Combining (3.2) and (3.4) then gives a single differential equation for $A_y(x)$ which can be solved numerically. This essentially completes the solution, for now one can obtain B_z from (3.4), ϕ from the formula for $\phi(A_y)$, E from $\phi(x)$, etc.

The procedure that we used to solve the more general set of Equations (3.1)-(3.5) etc.. is similar to that for the case considered by Sestero, except that we needed to use numerical methods more extensively. The root $\phi(A_y, A_z)$ of (3.6) was found by the method of successive approximations. With this, Q_i^{000}, Q_i^{001} were obtained by integrating the distribution function. Finally (3.1)-(3.4) were integrated by the classical predictor-corrector

numerical method, which gave numerically stable results that satisfied the total pressure balance condition (2.27). The numerical integration is to be started at a distance x_1 sufficiently far from the current sheet. At this distance the magnetic field components B_y and B_z are determined by the parameters B_1 and ϕ_1 defined by (2.12) and (2.13). Arbitrarily large negative values must also be given to $A_y(x_1)$ and $A_z(x_1)$, according to (2.14); $A_y(x_1) = -250\ B_1$ and $A_z(x_1) = \rho A_y(x_1)$ have proven to be sufficiently large values to require that the integration is started at a sufficiently large distance from the discontinuity surface. The parameter ρ (the ratio, A_z/A_y, of the two components of the vector potential at $x = x_1$) determines the rate of change of the magnetic field direction across the sheath. The value of ρ and of the other boundary conditions ($N_{l,i}$; $T_{l,i}$; B_l; ϕ_l; $N_{r,i}$; $T_{r,i}$) are given in the Table II for each model discussed in this paper.

4. SOLUTIONS

One can distinguish basically two different types of boundary layers - electron boundary layers whose thickness is on the order of a few electron gyroradii, and proton boundary layers whose thickness is on the order of a few proton gyroradii. Here we refer to an average gyroradius defined by

$$a = \frac{\sqrt{2km}}{2}\left[\frac{T_l^{1/2}}{B_l} + \frac{T_r^{1/2}}{B_r}\right], \qquad (3.7)$$

where the temperature refers to protons or electrons, as appropriate. Each type of boundary layer may appear in many different forms, depending on the boundary conditions and the nature of the distribution functions. The first two solutions that are discussed below illustrate electron boundary layers. The others illustrate different kinds of proton boundary layers. We stress that the results are illustrative, since measurements of boundary conditions and details of the distribution functions which are needed to completely specify real cases are not available. All of the results will be given in the dimensionless units listed in Table I. In particular, note that distance along the x-axis is scaled in 'electron skin depth' units (e.g.,

$\Delta x = 1$ for 2.37 km and 100 km corresponds to $\Delta x = 42$). The electron and proton gyroradii are probably more relevant, and these are shown for reference in the top panel in each of the figures to be discussed.

4.1. Electron boundary layers

Figure 2 illustrates the solutions corresponding to the boundary conditions given in columns (a) and (b) of Table II. In these examples, the direction of **B** changes across the layer, from $\phi_l = -45^0$ to $\phi_r = -18^0$ in model (a) and to $\phi_r = -63.3^0$ in model (b), and the magnetic field intensity increases from $B_l = 2\gamma$ to $B_r = 4.62\gamma$ in model (a) and to $B_r = 3.89\gamma$ in model (b). The number density $n_e = n_p$ decreases from $n_{e,p}(-\infty) = N_{l,ep} = 5\ cm^{-3}$ to $n_{e,p}(+\infty) = 2.5\ cm^{-3}$ in model (a) and to $n_{e,p}(+\infty) = 4.84\ cm^{-3}$ in model (b).

In the example on the left side of Figure 2, the electron temperature does not change ($T_{r,e} = T_{l,e}$ in model (a)). The current along $\hat{y}$ is driven primarily by a 'heat flux' due to a tail in the direction of the electron distribution function. The self-consistent electric field which drives the current, together with the corresponding potential and the charge separation, are shown in the top three panels of Figure 2. One can see from Figure 2 that the sheath does indeed have the dimensions of a few electron gyroradii. This is seen in the observables **B** and n and in the other quantities as well.

The electron drift speed, shown in the middle panel of Figure 2 together with the Alfvén speed, $V_A = B(\mu_o\ \Sigma n_i m_i)^{-1/2}$ in $(2kT_{l,e}/m_e)^{1/2}$ units, is particularly interesting. The electron drift speed exceeds the Alfvén speed in a narrow region on the order of four times the electron gyroradius, a_e, where most of the electron current is confined and where the largest change of the magnetic field occurs. Electrostatic instabilities are triggered when $W_e > V_A$ (Papadopoulos, 1973). Therefore, it is expected that the narrow current sheaths represented in Figure 2 will broaden rapidly by wave-particle interactions. This broadening of the electron current sheath will stop when the electron drift is reduced below the threshold for zero growth rate of the unstable modes. In this final situation the perpendicular electric field, E_x, will be significantly reduced and the total magnetic field variation

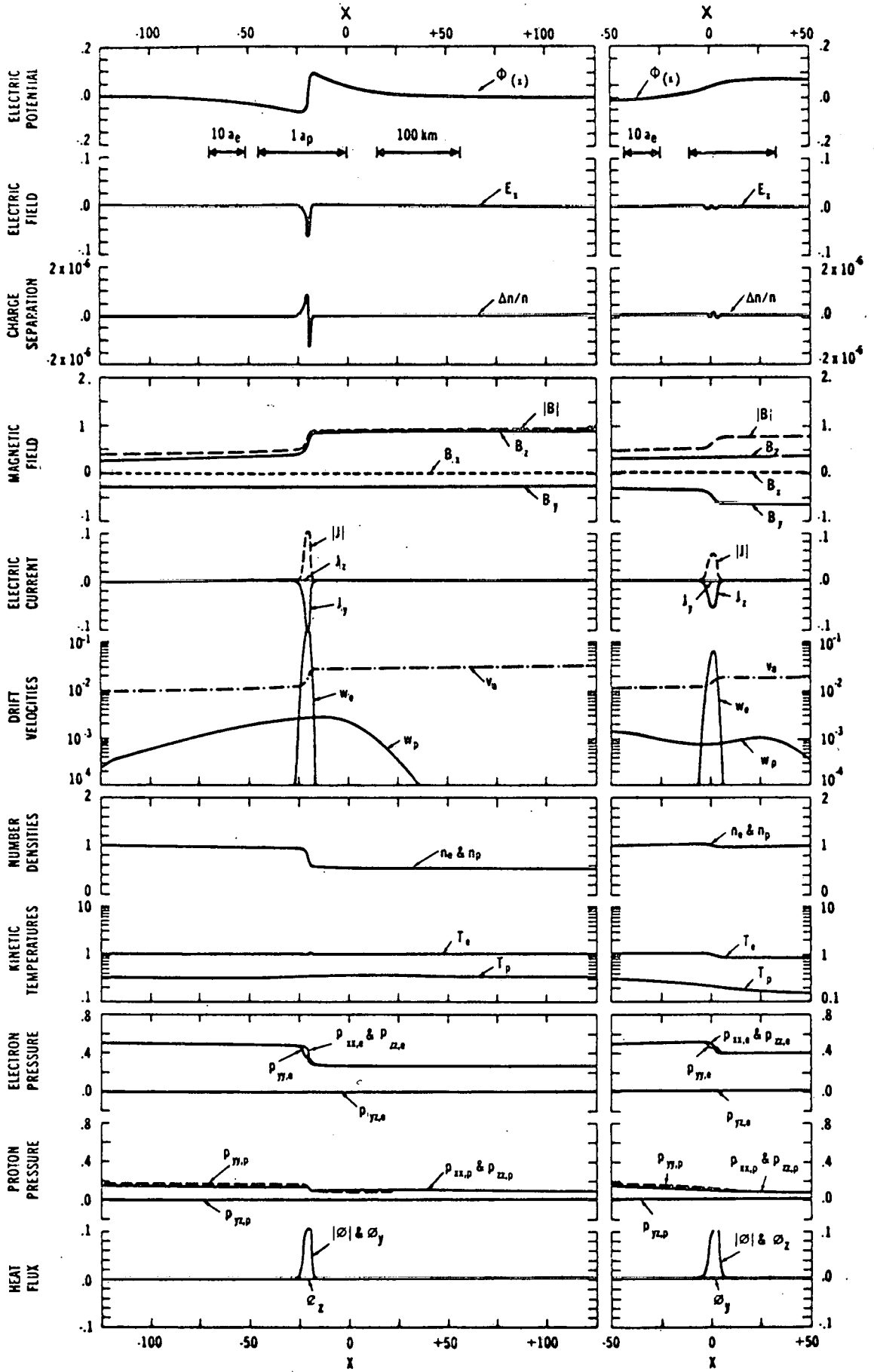
X
-100
-50
0
+50
+100
ELECTRIC POTENTIAL
Φ(x)
10 a_e
1 a_p
100 km
ELECTRIC FIELD
E_x
CHARGE SEPARATION
Δn/n
2 x 10^-6
MAGNETIC FIELD
|B|
B_z
B_x
B_y
ELECTRIC CURRENT
|J|
J_z
J_y
DRIFT VELOCITIES
v_e
w_e
w_p
NUMBER DENSITIES
n_e & n_p
KINETIC TEMPERATURES
T_e
T_p
ELECTRON PRESSURE
p_xx,e & p_zz,e
p_yy,e
p_yz,e
PROTON PRESSURE
p_yy,p
p_xx,p & p_zz,p
p_yz,p
HEAT FLUX
|Ø| & Ø_y
Ø_z
Ø_y

Fig. 2

will be spread over a distance larger than 4 electron gyroradii. During this transition period of pitch angle diffusion more electrons are scattered into trapped orbits. As a consequence the trapped particle population is changed as well as the electric potential distribution required to maintain the quasi- neutrality. The electron pitch angle distribution $f_e(v)$ becomes eventually more isotropic inside the sheath. Therefore, narrow current sheaths like that illustrated in Figure 2 are highly unstable and will evolve in a short time toward broader ones for which the electrons may still be the electric current carriers but in which their drift velocity W_e doesn't exceed the Alfvén speed V_A. When this stage is reached, the much slower Coulomb collisions will broaden it even more. Since the electron Coulomb collision time is only one day at 1 AU, it is expected that the electron velocity distribution reaches rapidly an equilibrium state where it is nearly isotropic and where the electrons no longer carry the electric current responsible for the most commonly observed large tangential discontinuities in the solar wind. Note that if electron sheaths with a thickness of only 4 electron gyroradii were present in the solar wind, they should be seen in the high resolution magnetograms as large amplitude changes in B_y and B_z over a period of 0.1 s, close to the time resolution of the IMP I magnetometer (0.08 s). Among the 400 directional discontinuities that we examined (Burlaga *et al.*, 1976) *none* had a thickness comparable to that expected for an electron sheath. This can be considered as evidence for a mechanism such as that just discussed, which can destroy an electron sheath in a time less than the transit time of the solar wind between the Sun and 1 AU.

The event shown on the right-hand side of Figure 2 (model (b)) is similar to that which we have been discussing except that the distribution function is now chosen such that both the electron and proton temperatures change across the layer (see Table II). This does not alter rhe essential features of the structure. Again the width is on the order of several a_e, and the drift speed W_e exceeds the Alfvén speed. It too is probably unstable and it is not likely to be observed in the solar wind.

4.2. Proton boundary layers

For simplicity, we shall assume in the following discussion of proton boundary layers that the electron velocity distribution is an isotropic maxwellian function throughout the boundary layer - i.e., that the electron pressure anisotropy is everywhere zero as well as the electron fluxes ($N_{l,e} \equiv N_{r,e}$; $T_{l,e,} \equiv T_{r,e}$ in Equation (2.34)). We shall further restrict the discussion to a two- component (proton and electron) plasma. In this case (3.6) can be solved explicitly for $\phi(+\infty)$ and $\phi(-\infty)$. In particular,

$$\phi(+\infty) = \frac{T_{r,e}T_{r,p}}{T_{l,e}(T_{r,e} + T_{r,p})} \ln\left(\frac{N_{r,p}}{N_{r,e}}\right) \quad ; \tag{4.1}$$

and a similar expression exists for $\phi(-\infty)$ where the subscript r is replaced by the subscript l. When $N_{l,p} \equiv N_{l,e}$, one finds that $\phi(-\infty) \equiv 0$. The value of $\phi(+\infty)$ is negative in the model (c) because $N_{r,p}/N_{r,e}$ is smaller than unity in Equation (4.1) (see Table II).

The electron and proton densities at $x = +\infty$ are given explicitly by

$$n_e(+\infty) = n_p(+\infty) = N_{r,p}^{[T_{r,p}/(T_{r,p} + T_{r,e})]} N_{r,e}^{[T_{r,e}/(T_{r,p} + T_{r,e})]} \quad ; \tag{4.2}$$

and a similar expression for $n_e(-\infty)$ and $n_p(-\infty)$ with the subscript r replaced by l. When $N_{l,p} \equiv N_{l,e}$, one finds that $n_e(-\infty) = n_p(-\infty) = N_{l,p}$. The values of $n_e(+\infty)$ (in cm^{-3}), and the value of $\phi(+\infty)$ (in volts) are given in Table II for each model.

From the total pressure balance Equation (2.27) one has the following equation which must be satisfied throughout the boundary layer

$$\sum_i p_{xx,i} + \frac{B^2}{2\mu_o} + \frac{\epsilon_o E^2}{2} = \text{const}, \tag{4.3}$$

where $p_{xx,i} = n_i k T_{xx,i}$. Various combinations of changes in n, T, and B across the boundary

layer are possible, and several will be considered below. We shall present plots of the proton drift speed, W_p, and the total proton heat flux, q. The y-component of the drift speed $W_{y,i}$ is related to the second and third order moments and to the electric field E_x, by

$$\frac{\partial Q^{210}}{\partial x} - \frac{Ze}{m}\,[nW_y E_x - B_z(Q^{200} - Q^{020}) - B_y Q^{011}] = 0 \qquad (4.4)$$

where Q^{200} and Q^{020} are related to the partial pressure tensor by

$$Q^{200} = \frac{p_{xx}}{m} = \frac{p_{xx}}{m} \quad , \qquad (4.5)$$

$$Q^{020} = \frac{p_{yy}}{m} + nW_y^2 = \frac{p_{yy}}{m} \quad , \qquad (4.6)$$

$$Q^{002} = \frac{p_{zz}}{m} + nW_z^2 = \frac{P_{zz}}{m} \quad , \qquad (4.7)$$

(the subscript i for the particle species is omitted in (4.4)-(4.7)). The heat flux components $q_{y,i}$ and $q_{z,i}$, are defined in terms of the third order moments by

$$q_y = m/2[Q^{210} + Q^{030} + Q^{013}] + mnW^2 W_y - W_x P_{xy} -$$

$$- W_y P_{yy} - W_z P_{zy} - \tfrac{1}{2} W_y [P_{yx} + P_{yy} + P_{zz}] \; ; \qquad (4.8)$$

and a similar expression for q_z.

Several self-consistent solutions of the boundary layer equations will now be discussed. First, we consider two cases in which both the magnetic field intensity and direction change, then we discuss two cases in which the magnitude but not the direction changes, and finally we present two cases in which the field direction but not the intensity changes across the boundary layer.

Figure 3a shows a situation in which the proton temperatures $T_{r,p}$ and $T_{l,p}$ are equal,

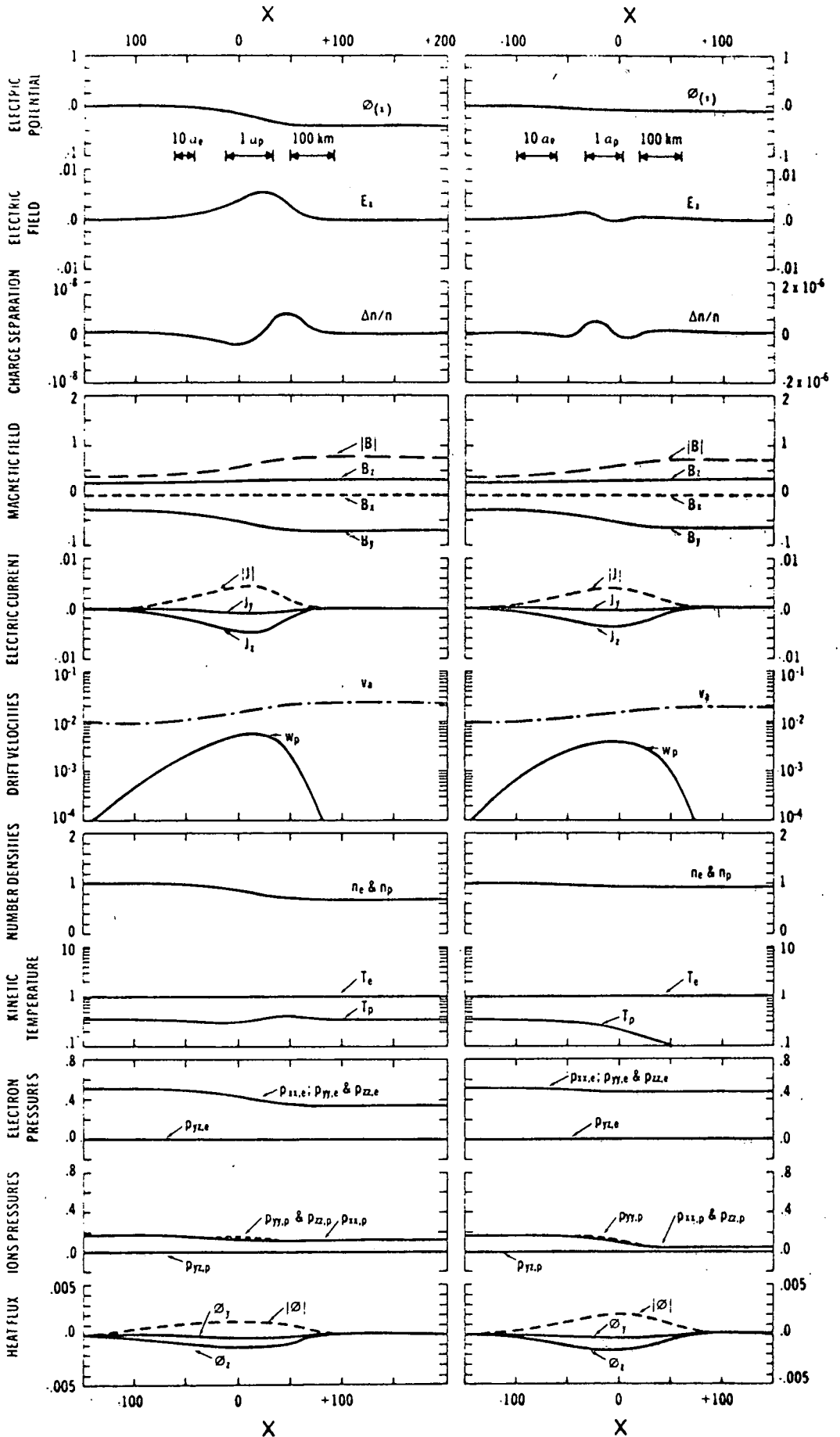
X
100
0
+100
+200
-100
ELECTRIC POTENTIAL
ELECTRIC FIELD
CHARGE SEPARATION
MAGNETIC FIELD
ELECTRIC CURRENT
DRIFT VELOCITIES
NUMBER DENSITIES
KINETIC TEMPERATURE
ELECTRON PRESSURES
IONS PRESSURES
HEAT FLUX
10 a_e
1 a_p
100 km
$\phi_{(x)}$
E_x
$\Delta n/n$
|B|
B_z
B_x
B_y
|J|
J_y
J_z
v_e
v_p
w_p
n_e & n_p
T_e
T_p
$p_{xx,e}$; $p_{yy,e}$ & $p_{zz,e}$
$p_{yz,e}$
$p_{yy,p}$ & $p_{zz,p}$
$p_{xx,p}$
$p_{yz,p}$
ϕ_y
$|\phi|$
ϕ_z

Fig. 3

and an increase in |B| is compensated by a decrease in density (model c in Table II). The field direction changes as well, and accordingly there are components of current along both $\hat{y}$ and $\hat{z}$. These are apparently due to a distortion in the proton distribution function which is equivalent to a heat flux. The resulting drift speed is less than the Alfvén speed, so the structure is expected to be stable. The width of the magnetic field transition is a few proton Larmor radii, consistent with the fact that the current is carried by protons which are gyrating and drifting in the magnetic and electric fields. The magnetic field intensity changes smoothly across the layer, consistent with the simple, single peaked current distribution.

The case (model (d)) in the right panel of Figure 3 is similar to the one just discussed, except that the proton temperature is assumed to decrease across the layer and thus a smaller drop in density is needed to compensate for the increase in |B|. The smaller change in density gives a smaller separation in charge density and a smaller change in electric field. Again, however, the current is mainly due to an equivalent heat flux in the proton velocity distribution, and the single hump in the current density gives a smooth transition in **B**. As in the previous case, the thickness of the boundary layer is a few proton gyroradii.

A somewhat more complicated boundary layer is shown in the left side of Figure 4 (model (e)). In this case, we assume that the magnetic field direction does not change, while the magnitude decreases across the boundary layer. The density is assumed to decrease only a little, and the decrease in n and |B| is balanced by an increase in T_p. In this case, the charge separations and changes in the electric field are small, and the boundary layer is broad, approximately $10a_p$. The current density and drift speed show a 3-humped structure which causes an irregular variation of |B| across the layer. The two large humps in J and W_p are probably due to the anisotropy in ion pressure, while the small hump seen in W_p is associated with a heat flux.

The event shown on the right of Figure 4 (model (f)) is similar to that just discussed in that the direction of **B** is constant throughout the layer while its magnitude increases. In this case, however, the change in density is assumed to be large. This large change is obtained by assuming that both T_p and |B| increase, so that both effects must be compensated for by a

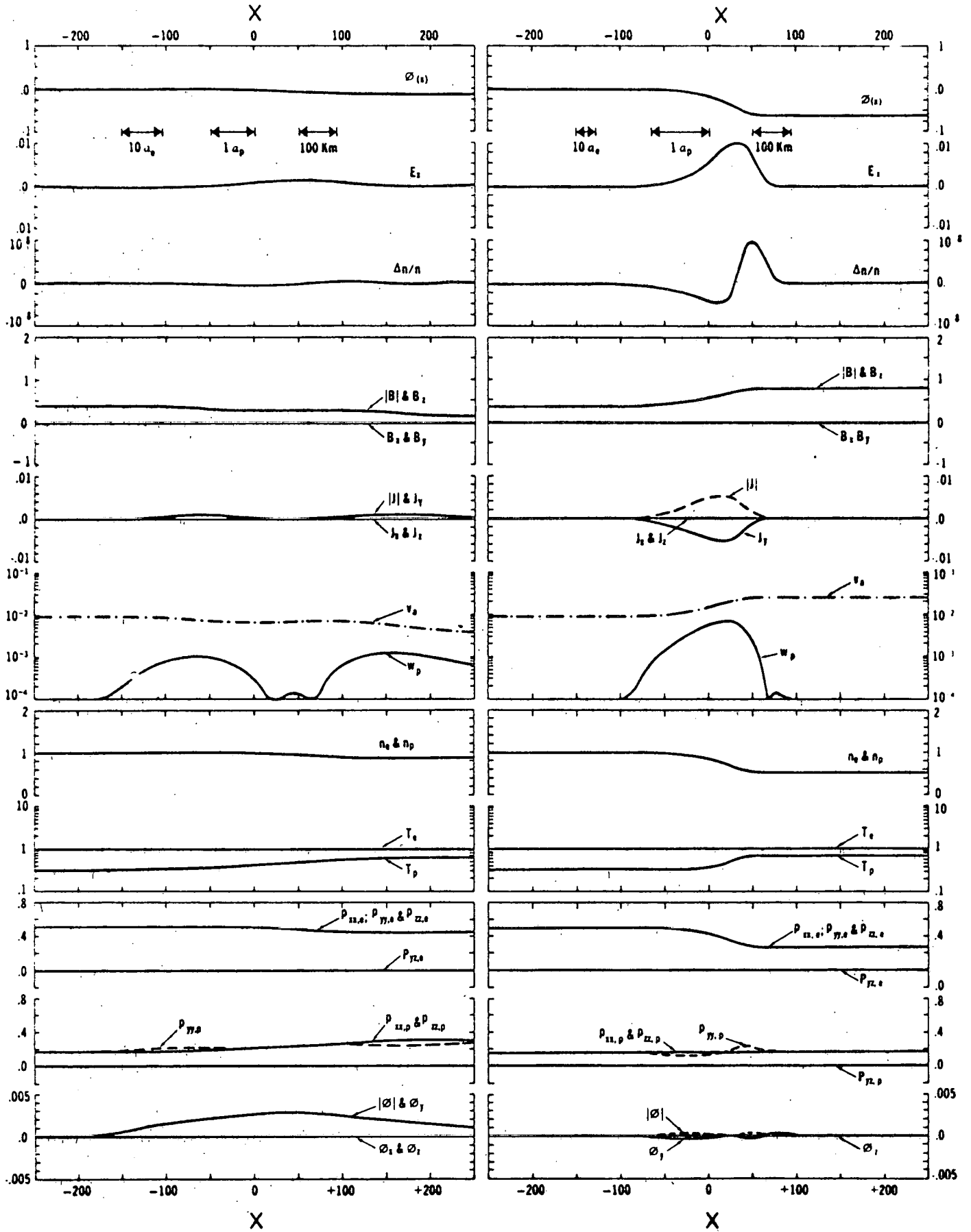
X
-200
-100
0
100
200
$\varnothing_{(x)}$
10 a_e
1 a_p
100 Km
E_x
$\Delta n/n$
$|B|$ & B_z
B_x & B_y
$|J|$ & J_y
J_x & J_z
v_e
w_p
n_e & n_p
T_e
T_p
$p_{xx,e}$; $p_{yy,e}$ & $p_{zz,e}$
$p_{yz,e}$
$p_{yy,p}$
$p_{xx,p}$ & $p_{zz,p}$
$p_{yz,p}$
$|\varnothing|$ & $\varnothing_y$
$\varnothing_x$ & $\varnothing_z$
$|\varnothing|$
$\varnothing_y$
$\varnothing_z$
+100
+200

Fig. 4

decrease in n_p in order to maintain pressure equilibrium. Because of the large density change, there is a larger charge separation and a larger change in E_x than in the previous case. The boundary layer is thinner, being only a few a_p in extent. The current density and W_p appear to have a relatively simple form, resulting in a smooth magnetic field transition, but the simplicity might be illusory, since there are significant changes in both the heat flux and anisotropies in the ion pressure.

Finally, let us consider two cases in which the magnetic field intensity is nearly constant but the direction changes by -9.8^0 and 8.6^0, respectively, across the boundary layer. The first case, shown in the left of Figure 5 (model (g)) is based on the assumption that there is a decrease in density which is balanced by an increase in T_p, with only a small change in $|\mathbf{B}|$. The charge separation and electric field change are extremely small ($< 10^{-2}$ mVm^{-1}; $\Delta n/n < 4 \times 10^{-9}$) the thickness of the layer is only $\approx 2a_p$. The current shows a single maximum, which is apparently due to an equivalent heat flux, and the variation in the field direction across the layer is accordingly uniform.

Model (h), on the right of Figure 5, is very similar to the preceding one; here the density increases while the temperature decreases, whereas in the preceding case the density decreases while the temperature increases. Again there are small changes in E_x and in the charge separation, the thickness is $\approx 2a_p$, the current density varies in a simple way and is related to the heat flux, and the field direction rotates by -8.6^0 uniformly across the layer.

All of the proton boundary layers discussed above have some features in common despite the variety of boundary conditions that were assumed. In every case, the thickness was greater than one Larmor radius, as one expects because the currents are due to gyrating protons. The thickness is always on the order of a few a_p, consistent with the observations of Burlaga *et al.* (1976). The drift speed of the gyrating protons that carry the current is always less than the Alfvén speed, consistent with the apparent stability of the boundary layers that are observed.

The currents in the case that the field changes only in direction are an order of magnitude smaller than those associated with changes in field intensity, but in both cases

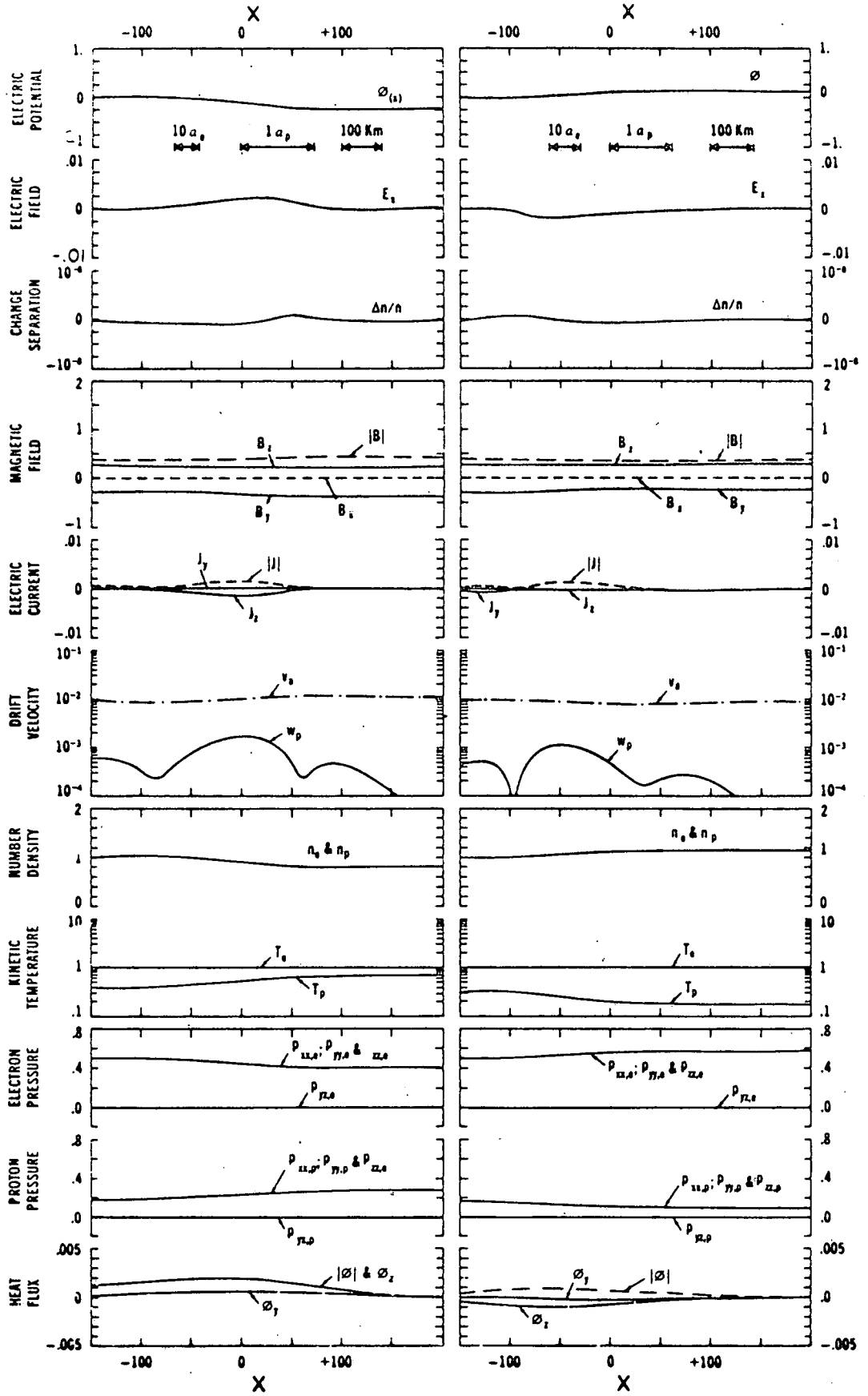
X
-100
0
+100
ELECTRIC POTENTIAL
ELECTRIC FIELD
CHARGE SEPARATION
MAGNETIC FIELD
ELECTRIC CURRENT
DRIFT VELOCITY
NUMBER DENSITY
KINETIC TEMPERATURE
ELECTRON PRESSURE
PROTON PRESSURE
HEAT FLUX
10 a_e
1 a_p
100 Km
$\Delta n/n$
n_e & n_p

Fig. 5

the current densities are much smaller for the proton boundary layers than for the electron boundary layers discussed earlier. In fact, the ratio of peak electron to peak proton current density is approximately the ratio of the corresponding thermal speeds, viz.,$((T_e/T_p)/-(m_e/m_p))^{1/2} \approx 70$. However, the smaller proton currents are spread over a layer which is thicker than the electron boundary layer; it is thicker by a factor equal to the ratio of the gyroradii of the protons and of the electrons, viz. $((T_p/T_e)/(m_e/m_p))^{1/2} \approx 25$, so the total current, $I = \int_{-\infty}^{\infty} J\, dx$, is of the same order of magnitude in both cases. It can be shown that each type of charged particles contributes to the total value of I_y (and I_z) by an amount proportional to $|Z_i|\beta_i$ averaged over the current layer. ($|Z_i|$ is the charge number, and β_i is the ratio of partial kinetic pressure $n_i kT_i$, and the magnetic pressure $B^2/2\mu_o$). Since $\Delta B_y = \mu_o I_z$ and $\Delta B_z = -\mu_o I_y$ the total jump in the magnetic field components across a tangential discontinuity is expected to be approximately proportional to $<\Sigma_i |Z_i|\beta_i>$, where the brackets mean the average value over the whole layer (i.e., $<A> = \lim_{x\to\infty} \int_{-x}^{+x} A dx / \int_{-x}^{+x} dx$).

5. SUMMARY AND DISCUSSION

We have presented a theory for thin boundary layers associated with MHD 'discontinuities' in a collisionless plasma, such as those observed in the solar wind. Since the observed boundary layers have a thickness on the order of a few Larmor radii, a kinetic theory which includes the effects of particle orbits is appropriate. We take the Vlasov equation as our starting point - i.e., we assume that the plasma is indeed collisionless over the small scales in the boundary layer, and we assume that the particles interact only with the magnetic and electric fields. We obtain self-consistent solutions of the Vlasov equation and Maxwell's equations for stationary, one-dimensional configurations corresponding to several sets of boundary conditions. Our method, which is an extension of that used by Sestero (1964) to allow for changes in magnetic field direction and temperature, is basically the following. We choose a form of the distribution function which satisfies Vlasov's equation and reduces to a Maxwellian distribution at $\pm\infty$, and we integrate this to obtain ion and electron densities and currents which are functions of the electrostatic potential

$\phi(x)$ and the vector potential **A**. A and ϕ are related by an equation which is solved numerically by neglecting the charge separation to first approximation. The currents and densities are then introduced into Maxwell's equations for **B** which are integrated numerically to obtain a solution for A(x), from which all other relevant quantities can be computed.

Two kinds of boundary layers are possible. In one the current is carried by electrons, and in the other the current is carried by protons.

Two examples of electron boundary layers were discussed. In both cases, the thickness was on the order of a few electron Larmor radii, and the field changed smoothly across the layer. The drift speed was found to exceed the Alfvén speed in the boundary layer, and such a situation is unstable. Thus, such stationary boundary layers are not expected to be observed. In fact, no boundary layers with dimensions as thin as several electron gyroradii have been detected in the solar wind.

Several kinds of proton boundary layers were examined. We considered situations with both a change in magnetic field intensity and direction, with directional changes only, and with intensity changes only. In every case, the thickness was on the order of a few proton gyroradii and the magnetic field changed relatively smoothly through the layer. The thickness and variation did, however, depend somewhat on the boundary conditions. The drift speed was always less than the Alfvén speed, consistent with the fact that such structures are actually observed in the solar wind.

An infinite number of configurations is possible, corresponding to the number of boundary conditions that are allowed. It is not possible, perhaps not even important, to 'fit' in detail each and every boundary layer that is observed. Nevertheless, the solutions that we have presented illustrate the basic physics involved in these layers and our general conclusions are consistent with the general characteristics of the boundary layers most commonly observed in the solar wind near 1 AU.

The theory that we presented should be applicable to conditions that exist in the solar wind away from 1 AU. Thus, we expect that the thickness will always be found to be a few to several proton gyroradii. The gyroradius varies as $\sqrt{T/B}$. Little is known yet about T(r), but the magnetic field intensity is observed to change as predicted by Parker's model, being close to r^{-2} near the Sun and r^{-1} far beyond 1 AU. The temperature probably falls off less rapidly than the adiabatic rate, $T \sim r^{4/3}$. Thus, one expects the gyroradius and therefore the thickness of the boundary layers to increase with distance from the Sun. Particle and field measurements are needed to test this prediction. The preliminary Pioneer 10 results seem to be consistent with our theory in that an increase in thickness with distance has been reported (Tsurutani and Smith, 1975). However, the thickness in gyroradii has not yet been determined in that experiment. Similar studies are under way in the Helios and Mariner 10 data. If it is found that our theory is consistent with the observations we can assume that thickness is a few proton gyroradii as predicted, and then use the observed magnetic boundary layers as thermometers to determine the proton temperature. An extension of the theory predicted in this paper is needed to realize this application.

ACKNOWLEDGEMENTS

We thank D. Fairfield and L. Fisk for stimulating discussions. Programming support was provided by W. Mish and T. Carleton. One of us (J.L.) was supported by a National Academy of Sciences-National Research Council Resident Research Associateship. He thanks N. Ness and K. Ogilvie for their hospitality and support at the Laboratory for Extra-terrestrial Physics.

Appendix : Moments of the Velocity Distribution Function

Let us define the function of $f(p_y, p_z, W)$ by

$$f = N_l \left(\frac{m}{2\pi k T_l} \right)^{3/2} \exp \left(-\frac{W}{kT_l} \right) \eta(-p_y)\eta(-p_z) +$$

$$+ N_r \left(\frac{m}{2\pi k T_r} \right)^{3/2} \exp \left(-\frac{W}{kT_r} \right) [1 - \eta(-p_y)\eta(-p_z)] \qquad (A1)$$

where $\eta(p)$ is the step function equal to zero for $p < 0$, and equal to unity everywhere else. The function (A1) is a solution of the time independent Liouville or Vlasov's Equation (2.28), since it depends only on the constants of motion (2.29), (2.30) and (2.31).

When A_y and A_z, the components of the vector potential, are both equal to $-\infty$, $f(p_y, p_z, W)$ becomes an isotropic maxwellian velocity distribution with the characteristic temperature T_l, and density $N_l \exp[-Ze\phi(-\infty)/kT_l]$, where $\phi(-\infty)$ is the electric potential at $x = -\infty$, on the left-hand side of the tangential discontinuity ($\phi(-\infty) = 0$ according to Equation 2.17).

When A_y and/or A_z are equal to $+\infty$, $f(p_y, p_z, W)$ becomes again isotropic and maxwellian with a characteristic temperature, T_r, and density $N_r \exp[-Ze\phi(+\infty)/kT_r]$, where $\phi(+\infty)$ is the electric potential at $x = +\infty$ on the right-hand side of the discontinuity surface.

The integral of (A1) over the velocity space is a finite positive number, Q^{000}, and in general, any higher moment, Q^{smn} (Equation 2.22) of (A1) has a finite value as required for any velocity distribution function.

$$Q^{smn} = N_{l,e} \left(\frac{2kT_{l,e}}{m_e} \right)^{(m+n+s)/2} q^{smn} \qquad (A2)$$

$$q^{smn} = \frac{1}{8}\,\text{sign}(z)\,\mathcal{M}_s \left\{ n_l t_l \exp\left(-\frac{Z\phi}{t_l}\right) x \right.$$

$$x\ \mathcal{L}_m\left(\frac{|Z|\gamma a_y}{\sqrt{t_l}}\right)\mathcal{L}_n\left(\frac{|z|\gamma a_z}{\sqrt{t_l}}\right) + n_r t_r^{(m+n+s)/2} \exp\left(-\frac{Z\phi}{t_r}\right) x$$

$$\left. x\ \left[\mathcal{M}_m \mathcal{M}_n - \mathcal{L}_m\left(\frac{|Z|\gamma a_y}{\sqrt{t_r}}\right)\mathcal{L}_n\left(\frac{|Z|\gamma a_z}{\sqrt{t_r}}\right)\right]\right\} \qquad \text{(A3)}$$

Where $Z_i|e|$ is the electric charge and $m_i = m_e/\gamma^2$ the mass of the i-particles considered; a_y, a_z and ϕ are the dimensionless vector and scalar potentials depending on x; $n_{l,i} = N_{l,i}/N_{i,e}$; $n_{r,i} = N_{r,i}/N_{l,e}$; $t_{l,i} = T_{l,i}/T_{l,e}$; and $t_{r,i} = T_{r,i}/T_{l,e}$. The functions $\mathcal{L}_n$ and $\mathcal{M}_n$ are defined by

$$\mathcal{L}_n(x) = (-1)^n \frac{2}{\sqrt{\pi}} \int_x^\infty y^n e^{-y^2}\,dy$$

$$\mathcal{L}_o(x) = \text{Erfc}(x)$$

$$\mathcal{L}_1(x) = -\frac{1}{\sqrt{\pi}} e^{-x^2} \qquad \text{(A4)}$$

$$\mathcal{L}_2(x) = \frac{1}{\sqrt{\pi}} x\, e^{-x^2} + \frac{1}{2}\text{Erfc}(x)$$

$$\mathcal{L}_3(x) = -\frac{(1+x^2)}{\sqrt{\pi}} e^{-x^2} \text{ etc...}$$

where Erfc(x) is the complementary error function,

$$\mathcal{M}_n = [1 + (-1)^n] \frac{2}{\sqrt{\pi}} \int_o^\infty y^n e^{-y^2}\,dy \qquad \text{(A5)}$$

$$\mathcal{M}_0 = 2$$

$$\mathcal{M}_1 = 0$$

$\mathcal{U}_2 = 1$

$\mathcal{U}_3 = 0$ etc.

The dimensionless densities, fluxes, momentum flux tensors, energy fluxes are given by

$$n_i = q^{000} ; \tag{A6}$$

$$F_x = 0 ; \qquad F_y = q^{010} ; \qquad F_z = q^{001} ; \tag{A7}$$

$$P_{xx} = q^{200}/\gamma^2 ; \qquad P_{xy} = P_{xz} = 0 ; \tag{A8}$$

$$P_{yx} = 0 ; \qquad P_{yy} = q^{020}/\gamma^2 ; \qquad P_{yz} = q^{011}/\gamma^2 ; \tag{A9}$$

$$P_{zx} = 0 ; \qquad P_{zy} = q^{011}/\gamma^2 ; \qquad P_{zz} = q^{002}/\gamma^2 ; \tag{A10}$$

$$\epsilon_x = 0 ; \qquad \epsilon_y = (q^{210} + q^{030} + q^{012})/\gamma^2 ;$$

$$\epsilon_z = (q^{201} + q^{021} + q^{003})/\gamma^2 \text{ , etc.} \tag{A11}$$

The dimensional quantities are obtained from Table I. This set of moments satisfy necessarily the general transport equations (i.e., the Maxwell moments equations) deduced from Vlasov's equation (2.28).

It is obvious that (A1) is not a unique nor the most general solution of Vlasov's equation, but it is a function that satisfies the boundary conditions that we have imposed at $x = \pm \infty$.

Different temperature anisotropies ($T_{\parallel}/T_{\perp} \neq 1$) or/and non-zero bulk speeds (V_l, $V_r \neq 0$) on both sides of the discontinuity surface can be included in kinetic descriptions by appropriate choices of $f(p_y, p_z, W)$. Although these generalizations increase the complexity

of the mathematical expressions for $Q_i^{s\,m\,n}$, they can in principle be obtained and studied by the same kinetic method. Roth (1975, personal communication) has derived such a generalization to determine a minimum thickness of the plasmapause boundary when V_l and V_r are not equal to zero.

REFERENCES

ALPERS, W. : 1969, 'Steady state charge neural models of the magnetopause', *Astrophys. Space Sci.*, **5** , 425.

ALPERS, W. : 1971, 'On the equilibrium of an exact charge neutral magnetopause', *Astrophys. Space Sci.*, **11**, 471.

BURLAGA, L.F. : 1969, 'Directional discontinuities in the interplanetary magnetic field'. *Solar Phys.*, 7, 54.

BURLAGA, L.F. : 1971, 'Hydromagnetic waves and discontinuities in the solar wind', *Space Sci. Rev.*, **12**, 600.

BURLAGA, L.F. : 1972, 'Microstructure of the interplanetary medium', in C.P. Sonett, P.J. Coleman, Jr., and J.M. Wilcox (eds.), *The Solar Wind*, NASA SP-308.

BURLAGA, L.F. and Ness, N.F. : 1969, 'Tangential discontinuities in the solar wind', *Solar Phys.*, **9**, 467.

BURLAGA, L.F., LEMAIRE, J. and TURNER, J.M. : 1976, 'Interplanetary layers at IAU', (to be published).

PAPADOPOULOS, K. : 1973, 'Electrostatic turbulence at colliding plasma streams as the source of ion heating in the solar wind', *Astrophys.J.*, **179**, 931.

SESTERO, A. : 1964, 'Structure of plasma sheaths', *Physics of Fluids*, 7, 44.

SISCOE, G.L. : 1974, 'Discontinuities in the solar wind', in C.T. Russell (ed.), *Solar Wind Three*, Institute of Geophysics and Planetary Physics, Univ. of California, Los Angeles, 90024, p. 151.

SISCOE, G.L., DAVIS, L., Jr., COLEMAN, P.J., Jr., SMITH, E.J., and JONES, D.E. : 1968, 'Power spectra and discontinuities of the interplanetary magnetic field : Mariner 4'. *J. Geophys. Res.*, 73, 61.

SMITH, E.J. : 1973. 'Identification of interplanetary tangential and rotational discontinuities',*J. Geophys. Res.*, 78, 2088.

STERN, D.P. : 1975, 'Charged particle motions in a magnetic field that reduce to motions in a potential', *Am. J. Physics*, **43**, 689.

TSURUTANI, B.T. and SMITH, E.J. : 1975, 'Interplanetary discontinuities between 1 and 5 AU', *EOS Trans. AGU*, **56**, 1055.

100 - BIAUME, F., Détermination de la valeur absolue de l'absorption dans les bandes du système de Schumann-Runge de l'oxygène moléculaire, 1972.

101 - NICOLET, M. and W. PEETERMANS, The production of nitric oxide in the stratosphere by oxidations of nitrous oxide, 1972.

102 - VAN HEMELRIJCK, E. et H. DEBEHOGNE, Observations au Portugal de phénomènes lumineux se rapportant à une expérience de lâcher de barium dans la magnétosphère, 1972.

103 - NICOLET, M. et W. PEETERMANS, On the vertical distribution of carbon monoxide and methane in the stratosphere, 1972.

104 - KOCKARTS, G., Heat balance and thermal conduction, 1972.

105 - ACKERMAN, M. and C. MULLER, Stratospheric methane from infrared spectra, 1972.

106 - ACKERMAN, M. and C. MULLER, Stratospheric nitrogen dioxide from infrared absorption spectra, 1972.

107 - KOCKARTS, G., Absorption par l'oxygène moléculaire dans les bandes de Schumann-Runge, 1972.

108 - LEMAIRE, J. et M. SCHERER, Comportements asymptotiques d'un modèle cinétique du vent solaire, 1972.

109 - LEMAIRE, J. and M. SCHERER, Plasma sheet particle precipitation : A kinetic model, 1972.

110 - BRASSEUR, G. and S. CIESLIK, On the behavior of nitrogen oxides in the stratosphere, 1972.

111 - ACKERMAN, M. and P. SIMON, Rocket measurement of solar fluxes at 1216 Å, 1450 Å and 1710 Å, 1972.

112 - CIESLIK, S. and M. NICOLET, The aeronomic dissociation of nitric oxide, 1973.

113 - BRASSEUR, G. and M. NICOLET, Chemospheric processes of nitric oxide in the mesosphere and stratosphere, 1973.

114 - CIESLIK, S. et C. MULLER, Absorption raie par raie dans la bande fondamentale infrarouge du monoxyde d'azote, 1973.

115 - LEMAIRE, J. and M. SCHERER, Kinetic models of the solar and polar winds, 1973.

116 - NICOLET, M., La biosphère au service de l'atmosphère, 1973.

117 - BIAUME, F., Nitric acid vapor absorption cross section spectrum and its photodissociation in the stratosphere, 1973.

118 - BRASSEUR, G., Chemical kinetic in the stratosphere, 1973.

119 - KOCKARTS, G., Helium in the terrestrial atmosphere, 1973.

120 - ACKERMAN, M., J.C. FONTANELLA, D. FRIMOUT, A. GIRARD, L. GRAMONT, N. LOUISNARD, C. MULLER and D. NEVEJANS, Recent stratospheric spectra of NO and NO_2, 1973.

121 - NICOLET, M., An overview of aeronomic processes in the stratosphere and mesosphere, 1973.

122 - LEMAIRE, J., The "Roche-Limit" of ionospheric plasma and the formation of the plasmapause, 1973.

123 - SIMON, P., Balloon measurements of solar fluxes between 1960 Å and 2300 Å, 1974.

124 - ARIJS, E., Effusion of ions through small holes, 1974.

125 - NICOLET, M., Aëronomie, 1974.

126 - SIMON, P., Observation de l'absorption du rayonnement ultraviolet solaire par ballons stratosphériques, 1974.

127 - VERCHEVAL, J., Contribution à l'étude de l'atmosphère terrestre supérieure à partir de l'analyse orbitale des satellites, 1973.

128 - LEMAIRE, J. and M. SCHERER, Exospheric models of the topside ionosphere, 1974.

129 - ACKERMAN, M., Stratospheric water vapor from high resolution infrared spectra, 1974.

130 - ROTH, M., Generalized invariant for a charged particle interacting with a linearly polarized hydromagnetic plane wave, 1974.

131 - BOLIN, R.C., D. FRIMOUT and C.F. LILLIE, Absolute flux measurements in the rocket ultraviolet, 1974.

132 - MAIGNAN, M. et C. MULLER, Méthodes de calcul de spectres stratosphériques d'absorption infrarouge, 1974.

133 - ACKERMAN, M., J.C. FONTANELLA, D. FRIMOUT, A. GIRARD, N. LOUISNARD and C. MULLER, Simultaneous measurements of NO and NO_2 in the stratosphere, 1974.

134 - NICOLET, M., On the production of nitric oxide by cosmic rays in the mesosphere and stratosphere, 1974.

135 - LEMAIRE, J. and M. SCHERER, Ionosphere-plasmasheet field aligned currents and parallel electric fields, 1974.

136 - ACKERMAN, M., P. SIMON, U. von ZAHN and U. LAUX, Simultaneous upper air composition measurements by means of UV monochromator and mass spectrometer, 1974.

137 - KOCKARTS, G., Neutral atmosphere modeling, 1974.

138 - BARLIER, F., P. BAUER, C. JAECK, G. THUILLIER and G. KOCKARTS, North-South asymmetries in the thermosphere during the last maximum of the solar cycle, 1974.

139 - ROTH, M., The effects of field aligned ionization models on the electron densities and total flux tubes contents deduced by the method of whistler analysis, 1974.

140 - DA MATA, L., La transition de l'homosphère à l'hétérosphère de l'atmosphère terrestre, 1974.

141 - LEMAIRE, J. and R.J. HOCH, Stable auroral red arcs and their importance for the physics of the plasmapause region, 1975.

142 - ACKERMAN, M., NO, NO_2 and HNO_3 below 35 km in the atmosphere, 1975.

143 - LEMAIRE, J., The mechanisms of formation of the plasmapause, 1975.

144 - SCIALOM, G., C. TAIEB and G. KOCKARTS, Daytime valley in the F1 region observed by incoherent scatter, 1975.

145 - SIMON, P., Nouvelles mesures de l'ultraviolet solaire dans la stratosphère, 1975.

146 - BRASSEUR, G. et M. BERTIN, Un modèle bi-dimensionnel de la stratosphère, 1975.

147 - LEMAIRE, J. et M. SCHERER, Contribution à l'étude des ions dans l'ionosphère polaire, 1975.

148 - DEBEHOGNE, H. et E. VAN HEMELRIJCK, Etude par étoiles-tests de la réduction des clichés pris au moyen de la caméra de triangulation IAS, 1975.

149 - DEBEHOGNE, H. et E. VAN HEMELRIJCK, Méthode des moindres carrés appliquée à la réduction des clichés astrométriques, 1975.

150 - DEBEHOGNE, H. et E. VAN HEMELRIJCK, Contribution au problème de l'abérration différentielle, 1975.

151 - MULLER, C. and A.J. SAUVAL, The CO fundamental bands in the solar spectrum, 1975.

152 - VERCHEVAL, J., Un effet géomagnétique dans la thermosphère moyenne, 1975.

153 - AMAYENC, P., D. ALCAYDE and G. KOCKARTS, Solar extreme ultraviolet heating and dynamical processes in the mid-latitude thermosphere, 1975.

154 - ARIJS, E. and D. NEVEJANS, A programmable control unit for a balloon borne quadrupole mass spectrometer, 1975.

155 - VERCHEVAL, J., Variations of exospheric temperature and atmospheric composition between 150 and 1100 km in relation to the semi-annual effect, 1975.

156 - NICOLET, M., Stratospheric Ozone : An introduction to its study, 1975.

157 - WEILL, G., J. CHRISTOPHE, C. LIPPENS, M. ACKERMAN and Y. SAHAI, Stratospheric balloon observations of the southern intertropical arc of airglow in the southern american aera, 1976.

158 - ACKERMAN, M., D. FRIMOUT, M. GOTTIGNIES, C. MULLER, Stratospheric HCl from infrared spectra, 1976.

159 - NICOLET, M., Conscience scientifique face à l'environnement atmosphérique, 1976.

160 - KOCKARTS, G., Absorption and photodissociation in the Schumann-Runge bands of molecular oxygen in the terrestrial atmosphere, 1976.

161 - LEMAIRE, J., Steady state plasmapause positions deduced from McIlwain's electric field models, 1976.

162 - ROTH, M., The plasmapause as a plasma sheath : A minimum thickness, 1976.

163 - FRIMOUT, D., C. LIPPENS, P.C. SIMON, E. VAN HEMELRIJCK, E. VAN RANSBEECK et A. REHRI, Lâchers de monoxyde d'azote entre 80 et 105 km d'altitude. Description des charges utiles et des moyens d'observation, 1976.